Inversion-based imaging: from LSRTM to FWI imaging

Bin Wang[1*], Yang He[1], Jian Mao[1], Faqi Liu[1], Feng Hao[1], Yi Huang[1], Mike Perz[1] and Scott Michell[1] compare and contrast LSRTM and FWI and conclude that the process of generating the FWI-imaging essentially amounts to nonlinear, data-domain inversion.

Summary
Least Squares RTM (LSRTM) is a powerful inversion-based imaging algorithm which minimizes the data misfit between observed seismic recordings and forward-modelled synthetic data. The algorithm, which can be implemented in either data or image domains, carries a fundamental limitation because it is based on a linear inversion theory which cannot accommodate velocity refinement as part of its model update process. Successful application of LSRTM therefore requires highly accurate velocity information, and if the velocity model is in significant error, modelled events will not be aligned kinematically with the observed data, and the algorithm will tend to produce unsatisfactory results.

FWI is another inversion-based algorithm that enjoys widespread industry use. Unlike LSRTM, FWI poses its inverse problem within a non-linear framework whereby it updates the velocity model and associated wave paths throughout its iterative process, gradually aligning modelled events with observed events. With the recent convergence of FWI and LSRTM methodologies, FWI is not only being used as a velocity update tool, but also as a direct imaging tool, thereby achieving two key imaging goals, namely refining the velocity model and deriving a better-quality seismic image. The latter process, which is known as 'FWI imaging', has recently been gaining a lot of industry attention as it offers the possibility of high-quality imaging along with workflow simplification.

In this article we will compare and contrast LSRTM and FWI. We conclude that the process of generating the FWI-imaging essentially amounts to nonlinear, data-domain inversion. This recognition facilitates a ready comparison against the data-domain form of LSRTM, the latter being a linear, data-domain inversion.

Introduction
Since the early 1990s, academic efforts aimed at improving image quality have been focusing on inversion-based algorithms, all of which are generally termed Least Squares Migration (LSM) (Schuster, 1993; Nemeth, et al, 1999). Figure 1 provides a brief history of the evolution of LSM up to the present time. While the initial effort of LSM was on post-stack imaging, it later shifted to the prestack domain (Yu et al, 2003; Dai and Schuster, 2009; Tang, 2009). In the early 2010s, the industry started to apply LSM algorithms to real data and observed improved imaging quality (Dong et al, 2012; Dai et al, 2013; Wang, 2014; Zeng, et al, 2014; Zhang et al, 2015). While early application of LSM was aimed at improving structural imaging on the migrated stack, industry demands later shifted the focus to LSM gathers and included the requirement that the gathers be AVO-compliant. To accommodate these differing needs, two classes of LSM algorithms have emerged from the above research efforts, namely data-domain LSM and image-domain LSM (Fletcher et al, 2016; Wang et al, 2016; Zeng et al, 2016). In more recent years, least squares

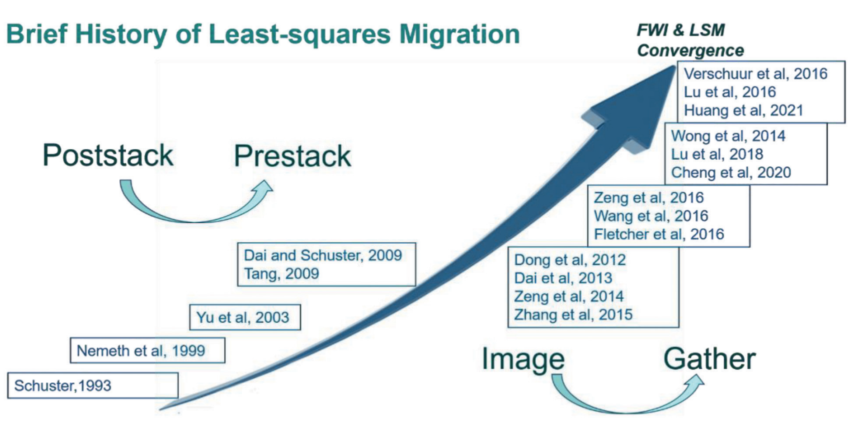

Figure 1 Brief evolution history of Least Squares Migration.

[1] TGS
[*] Corresponding author, E-mail: Bin.Wang@tgs.com
DOI: 10.3997/1365-2397.fb2021096

migrations have been applied for multiple imaging (Wong et al, 2014; Lu et al, 2018; Cheng et al, 2020).

Full waveform inversion (FWI) (Tarantola, 1984; Pratt et al, 1998; Sheng et al, 2006; Virieux and Operto, 2009; Warner et al, 2013) has developed over the years to provide a high-resolution velocity update which is more conformable with geological structures. FWI seeks an optimized solution by minimizing the differences between recorded and synthetic seismic data, but when the time shifts between the two datasets are larger than half of one cycle it can prevent convergence to a global minimum; it converges to a local minimum instead. To mitigate this cycle skipping problem, a reflection tomography model can be used as the FWI initial model with inversion starting from a low frequency and gradually increasing to higher frequencies, or other objective functions can be adopted which are less affected by cycle-skipping: Laplacian-Fourier domain FWI (Shin and Cha, 2009), reflection travel time inversion with dynamic warping (Ma et al, 2012; Ma and Hale, 2013), envelope inversion (Wu et al, 2014), adaptive waveform inversion (Warner, et al 2016), and time-lag FWI (Wang et al, 2019). Dynamic matching FWI (Mao et al, 2020) has proved to be a robust FWI algorithm for high-resolution model building. Because of these successful mitigation schemes for avoiding cycle skip, FWI is widely used to resolve challenging issues in velocity model building in complex geological settings, such as refining salt geometry (Michell et al, 2017; Xing et al, 2020; Huang et al, 2021). Another new recent development of high-frequency FWI is FWI imaging (Zhang et al, 2020; Wang et al, 2020; He, et al, 2021), which is discussed in more detail in this article.

Image-domain vs data-domain LSRTM

To meet different needs, two different types of LSRTM algorithms have been developed and used in the industry: 1) Data-domain LSRTM; and 2) Image-domain LSRTM.

As illustrated by Figure 2, the objective function of LSRTM is to minimize the data residual in L2 norm: $\|Lm - d\|^2$, where **L** is the forward modelling operator, **m** is the reflectivity model (a high resolution image), which will be inverted and $\boldsymbol{d}$ is the observed seismic data. Typically, the data is input as shot gathers and for each input record a shot-based Born modelling is applied to generate the synthetic seismic data. For data domain LSRTM, synthetic shots are compared with the observed shots trace by trace to get data residuals, to which RTM will be performed, where the reflectivity update will be obtained after proper scaling. This demigration (Born modelling) and migration process are kept iterating until the data residual is insignificant or meets the stopping criteria. Comparing with regular RTM, data-domain LSRTM gradually refines the image by

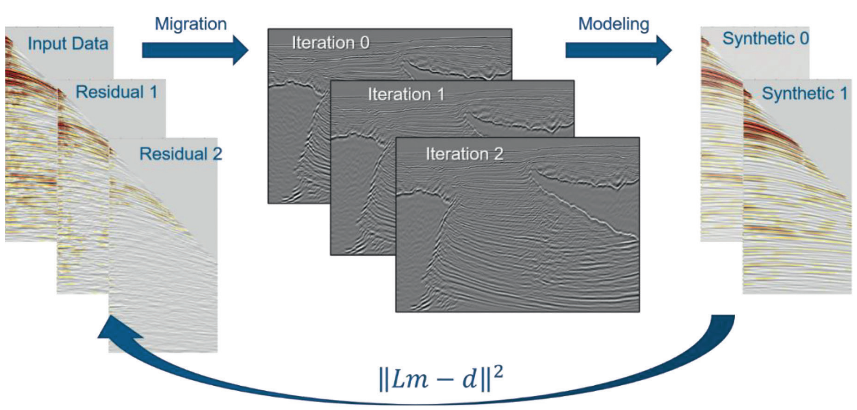

Figure 2 Schematic diagram illustrating data-domain LSM.

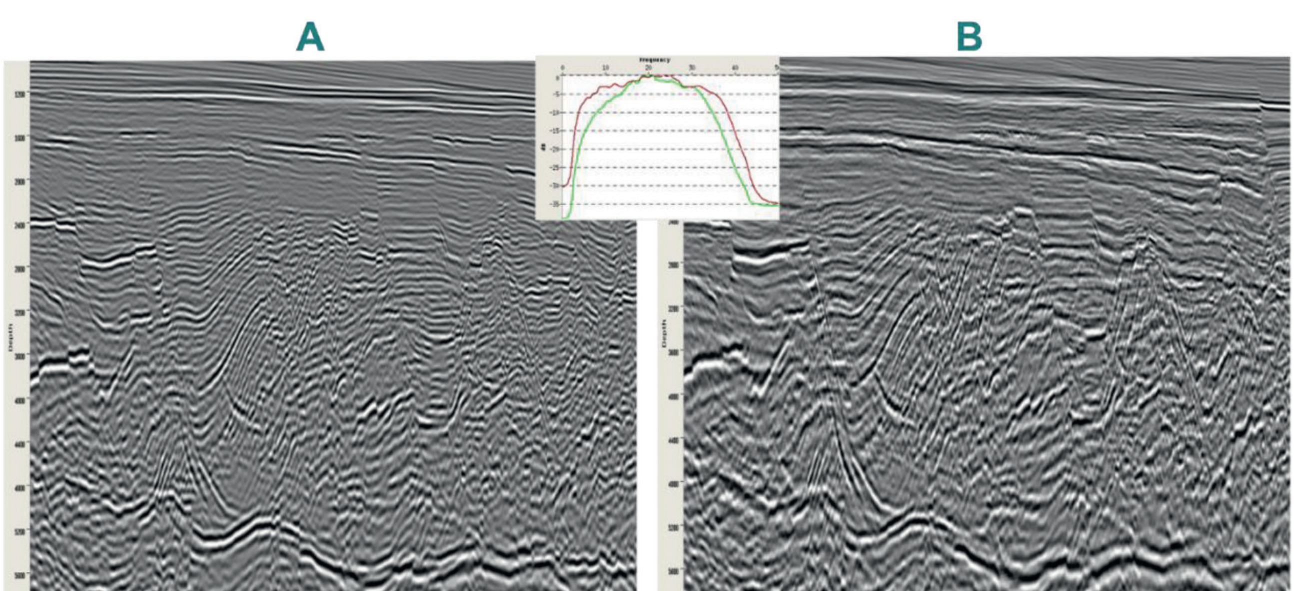

Figure 3 (A) regular RTM image; (B) Data-domain LSRTM image of same input as Figure 3A.

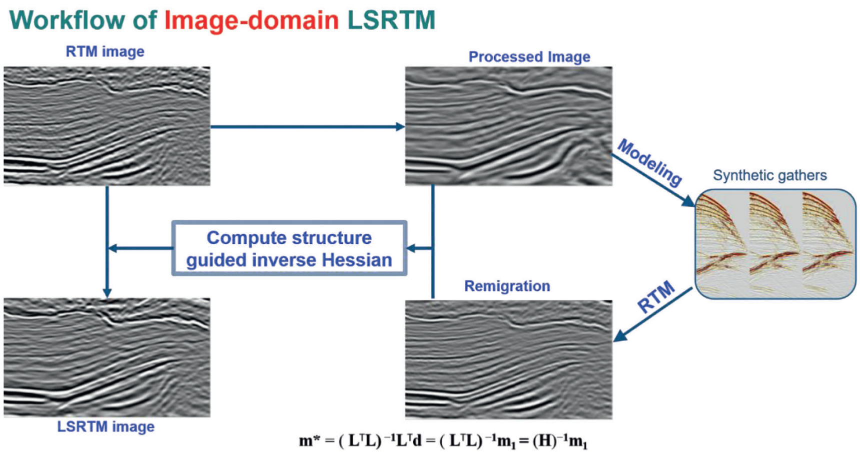

Figure 4 Schematic diagram illustrating image-domain LSRTM.

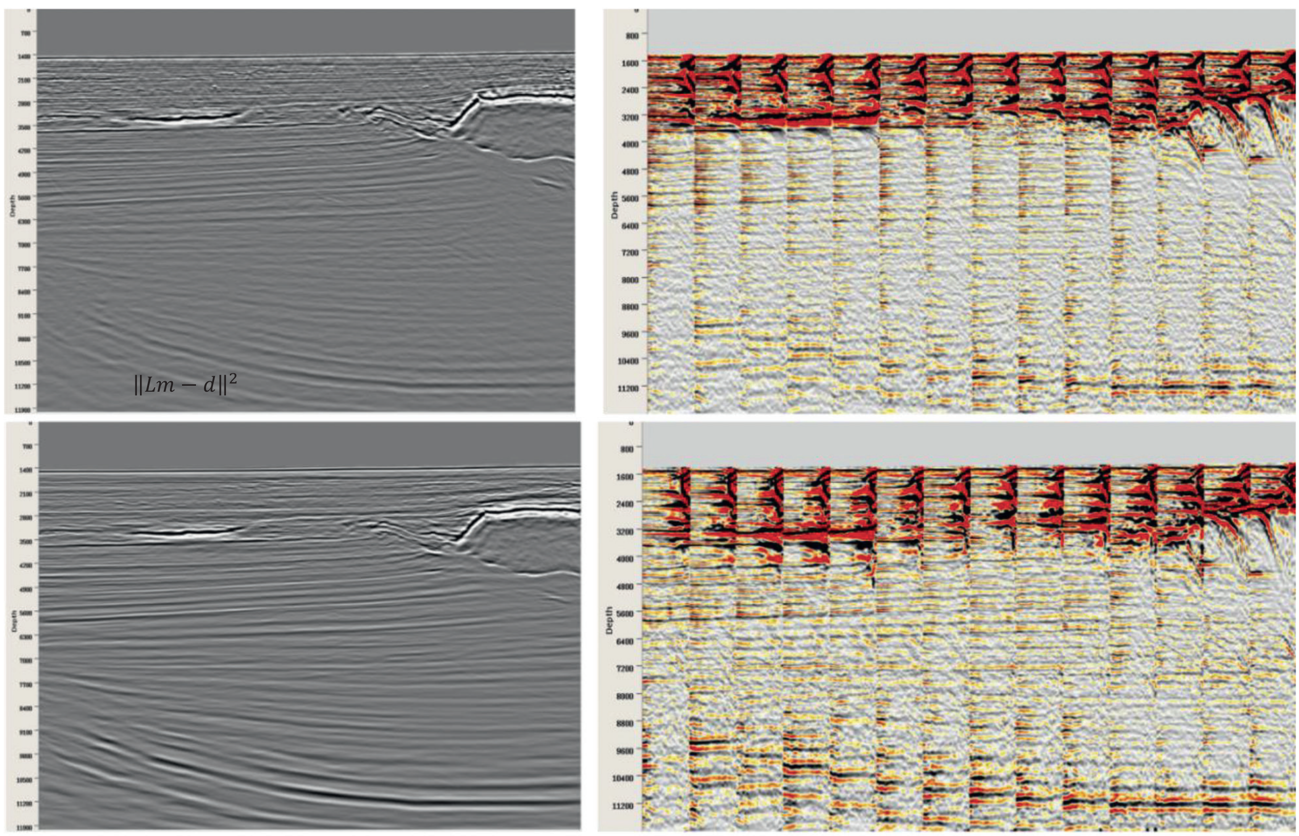

Figure 5 Left shows the migration stacked images, and right shows the migration gathers. The upper row is the regular RTM result, and the bottom row is the image-domain LSRTM result.

additional residual imaging, and each iteration hopefully adds more detail to the final image and ultimately produces an image with high resolution and quality.

Figure 3B shows an early example of data-domain LSRTM image. Compared with conventional RTM images conventional RTM image (Figure 3A), data-domain LSRTM can improve the focusing and coherency of events (Wang, 2014). The inversion image is more broadband, which is also indicated by the spectrum comparison, showing spectrum expansion at both the low and high-frequency ends (the green curve is for RTM and the red curve is for LSRTM). In particular, data-domain LSRTM is very effective at enhancing low frequencies, which is helpful to improve steep-dip events such as steep-dip faults.

Data-domain LSRTM is an iterative approach, typically requiring many iterations to converge, which can be expensive. Another shortcoming of the data domain approach is its non-effectiveness to balance the amplitude due to non-uniform illumination. To improve amplitude fidelity of the final image, and generate LSM gathers, image-domain LSRTM has been proposed and widely applied.

The image-domain LSM is based on the direct solution to the L2 norm-based objective function of least squares migration which is formulated as $\mathbf{m^*} = (\mathbf{H})^{-1}\mathbf{m}$, where $\mathbf{m}$ is the regular RTM image, and $\mathbf{m^*}$ is the image-domain LSRTM image. The difference between these two is the Hessian inverse $(\mathbf{H})^{-1}$. Image-domain LSRTM is typically a single iteration approach.

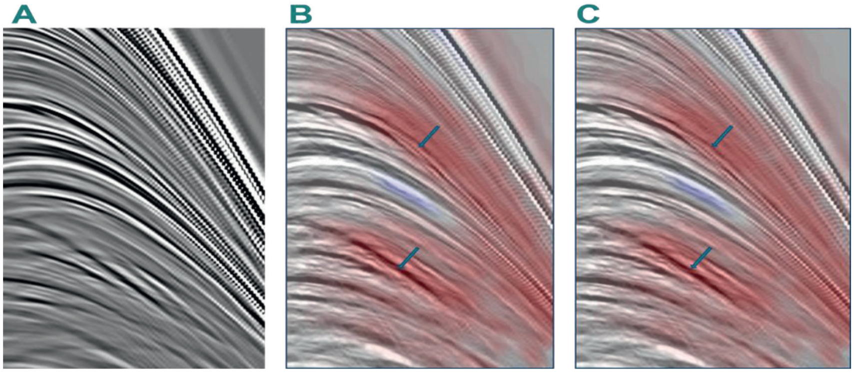

Figure 6 (A) synthetic shot created by Born modelling; (B) Observed shot before dynamic warping; (C) observed shot after dynamic warping to the synthetic shot.

There are different ways to approximate the Hessian operator: 1) A point-spreading function (PFS) based approach (Fletcher et al, 2016); and 2) A reflectivity-based approach (Wang et al, 2016; Zeng et al, 2016). Additionally, image-domain LSRTM can be integrated with data-domain LSRTM to make a hybrid approach to combine the advantages of both algorithms.

In this article, we briefly describe the reflectivity-based image-domain LSRTM. Referring to Figure 4, the upper-left image is the regular RTM image. To start the image-domain LSRTM, post-migration processing is first applied to the final RTM image to create an initial reflectivity image which has higher S/N and more balanced amplitude (shown upper-right in Figure 4), in which a round-trip of demigration (Born modelling) followed by remigration of the synthetic data is applied to generate an image. During the Born modelling, the same acquisition geometry as the original data is used to simulate the real and imperfect acquisition. After getting the new remigration image (shown at the lower-right image in Figure 4), an inverse matching filter is designed which matches the remigrated image to the initial reflectivity image and is used to approximate the inverse Hessian operation. Then the obtained inverse Hessian filter is applied to the original RTM image (upper left) to get the image-domain LSRTM image (at lower left in Figure 4).

Two important pieces of information are revealed by comparing the initial reflectivity image (upper right), with the remigration image (lower right): 1) amplitude changes (due to illumination issues) and 2) migration artifacts (due to imperfect acquisition or propagation effects from a complex velocity model such as salt body). The inverse matching filters effectively use these two pieces of information to achieve amplitude compensation, and therefore improve amplitude fidelity of the final image and remove/reduce migration artifacts and improve coherency and S/N of the final image.

Figure 5 shows an example of image-domain LSRTM. As compared with the regular RTM result (upper row), the image domain LSRTM (bottom row) can reduce the migration artifacts, boost weak subsalt signals, and the stack image is more coherent with better S/N ratio and more balanced amplitudes. For this example, two shallow salt bodies can be seen in the stacked images; the small shallow salt body on the left and the large salt body on the right. Due to illumination effects of the salt, in the subsalt area the amplitude is not balanced, especially in the migration gathers. More near-offset energy is penetrating through between the salts and more energy is blocked by the salt bodies at the far offset. The image-domain LSRTM can effectively compensate the amplitude due to non-uniform illumination, therefore improving the AVO fidelity.

Challenges of data-domain LSRTM

Data-domain LSRTM is an iterative data-fitting process. The objective is to fit the synthetic data, which is modelled using the current reflectivity model and the latest velocity model, to the observed data. It is a linear algorithm because the inverted result is the reflectivity model, not the velocity model. During iterations, the velocity model is fixed, so the wave propagation paths are not changed during the iterative process. The underlying fundamental assumption is that the velocity model is accurate, and kinematically the modelled synthetic events align with the observed events.

However, in the case where the velocity model contains significant errors, the synthetic data will not be able to kinematically align with the observed data, and the misfit will increase as offset increases. In such cases, the objective to reduce residual by iterating the process will not converge as the velocity is unchanged from one iteration to another.

To mitigate the non-convergence issue created by velocity errors, an algorithm called adaptive LSRTM was developed (Zeng et al, 2016). The basic idea is to align an observed event to the synthetic event by dynamic warping. As shown in Figure 6, due to velocity errors, the modelled events do not align with the observed ones as indicated by the arrows. Dynamic warping was applied to align the observed shot gather to the synthetic shot. The coloured background is the amount of time shift needed to align the two datasets. Using the warped input to replace the original observed shots, LSRTM can converge better. Figure 7 is an example which shows this adaptive LSRTM strategy can enable the convergence and improve image quality.

Though adaptive data-domain LSRTM can help to improve convergence, the process modifies the observed data to better fit the synthetic data (i.e., rather than the other way around), and is thus consistent with the current, erroneous, velocity model. A more natural way to enable the convergence is to update the velocity model itself so that the synthetic data kinematics are modified to fit those of the observed data.

Convergence of LSRTM and FWI

There are two major steps for depth imaging: 1) Velocity model building; 2) depth migration. FWI has been widely used as an inversion-based velocity update tool, while the counterpart for depth migration side is the data-domain LSRTM. There is a clear trend of convergence of these two inversion-based algorithms.

For FWI, it is used not only for velocity model building, the high-frequency FWI result is now beyond just providing a velocity model for depth imaging but also serves as an interpretable product itself. On the other hand, to resolve the non-convergence issue of linearized data-domain LSRTM, as discussed in the last section, we need a non-linear version of data-domain LSRTM, which is able to update the velocity model to change the kinematic information, in order for synthetic data to fit the observed data.

There are a few visible efforts seeking the convergence and integration of these two closely related technologies. Verschuur et al (2016) proposes Joint Migration Inversion (JMI), in which they propose to alternatively update the velocity model and reflectivity image. Lu et al (2016) advocated high-frequency FWI for inversion beyond velocity, and use FWI for impedance inversion. Zhang et al (2014) approached this problem from a true amplitude migration and inversion perspective, for velocity, impedance, and reflectivity inversion, concluding that for reflection data, near offset data provide information for impedance inversion and far offset data provide information for velocity inversion. More recently, a few groups demonstrated that FWI imaging, which is the normal derivative of the high-resolution velocity model derived by high-frequency FWI (Huang et al, 2021), is itself an excellent imaging tool.

Data-domain LSRTM and FWI have very similar data flows as illustrated in Figure 8. Both flows use shot gathers as input, both perform forward modelling to generate synthetic data, and both try to minimize the data misfit between observed data and synthetic data. However, there are several key differences between them. First, the inversion model is different: LSRTM seeks to update the reflectivity model, while FWI tries to update the velocity model. Second, the forward modelling is different: LSRTM performs reflectivity-based Born modelling and typically excludes surface multiples, while FWI performs a more accurate acoustic modelling and has the ability to include surface multiples. Third, LSRTM, like RTM, only uses the reflection mode as input, while FWI can accommodate diverse propagation modes (i.e., diving waves, primary reflections, multiple reflections etc). Finally, the non-linear nature of the FWI inverse problem requires a multi-band approach in which multiple passes of FWI are performed, each stepping from low to successively higher frequencies, and each using the final model of the former pass as its initial model (by contrast the linear LSRTM process performs a single band inversion which simultaneously incorporates information from all frequencies).

From Figure 8 it should be apparent that there are strong analogues between FWI imaging and LSRTM at all stages except at the end where FWI imaging requires an additional step, namely computation of the normal derivative of the final velocity model. If we consider the existence of this additional step alongside the algorithmic differences articulated in the previous paragraph, we can make some informed conjectures about why FWI imaging often seems to provide superior resolution relative to data-domain LSRTM, even when both are inverting the same input data set, and even in cases where the velocity model is believed to be known with good accuracy (and thus where the 'velocity-update' advantage of FWI imaging should not be significant). First, we note that FWI's differentiation step (which amounts to ***jw*** filtering in the frequency domain) does a high-end spectral shaping which ensures good support at high frequencies. While this differentiation process helps to emphasize the high frequencies relative to lows, it is obviously incapable of altering the fundamental high-frequency information content present in the input data, and so in theory cannot improve resolution over the LSRTM output. Still, we posit that the high-frequency emphasis afforded by differentiation provides a practical advantage by removing the need for any ex post facto processing which might be required on the LSRTM image (e.g, cosmetic wavelet processing). Second, the multi-band approach inherent in FWI allows the user to select a relatively coarse propagation grid for the low-frequency bands (propagation grid size is governed by stability and dispersion noise constraints and depends inversely on maximum frequency present in the passband under consideration), thereby allowing the use of a very high number of internal iterations in the data-fitting process and ultimately providing a very high-quality image at the low frequencies (note that these low-frequency Fourier components play an important role in steep-dip resolution). By contrast, LSRTM's single-pass approach requires a very fine propagation grid as dictated by the maximum frequency present in the data, and the computational expense associated with this fine grid poses a practical limitation on the number of internal algorithm iterations which can be used

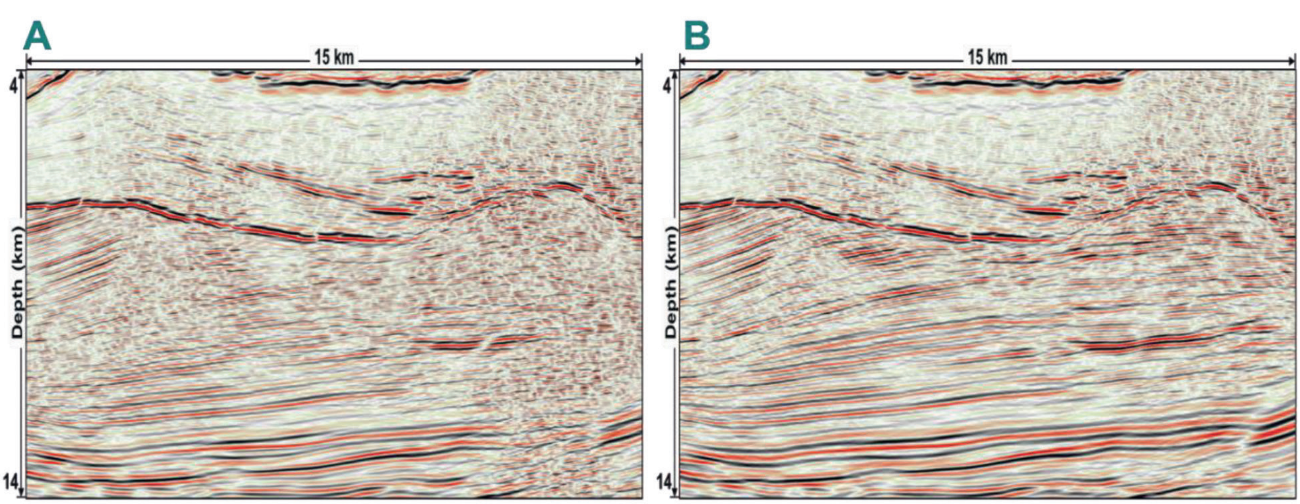

Figure 7 (A) regular RTM image; (B) Adaptive LSRTM image.

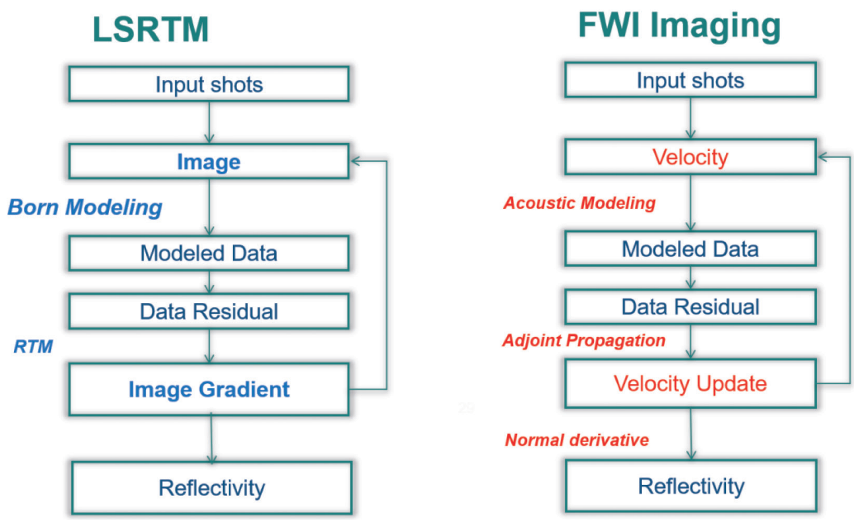

Figure 8 Comparison of LSRTM flow and data-domain FWI imaging flow.

for refining the model (of course FWI requires use of that same very fine propagation grid, but only for its final multi-band pass). A third explanation for the observation of superior resolution after FWI imaging lies in a practical nuance associated with the Born modelling step in LSRTM. The wavefield convolution with reflectivity model in Born modelling serves as a bandpass filtering. While in principle the reflectivity model can be captured with high accuracy through use of a very small numerical grid (i.e, typically much smaller than propagation grid), in practice efficiency considerations dictate that this grid size be selected to be larger than that which is required for complete capture of the reflectivity information. This 'reflectivity aliasing' can give rise to smearing in the final image. By contrast the acoustic modelling approach used in FWI does not require specification of a reflectivity model and so does not suffer from this smearing effect.

FWI imaging data examples

In this section, we show two real data examples of FWI imaging to demonstrate its usefulness. One example is from the US Gulf of Mexico and another is from the North Sea.

Sparse OBN survey in deep-water Gulf of Mexico: A large-scale sparse node survey called Amendment was conducted in the Gulf of Mexico in 2019. About 3000 nodes, spaced at 1000 m by 1000 m were deployed, with a source spacing of 50 m by 100 m. The programme was designed to acquire extra-long offset node data, with the objective of using FWI to derive a better velocity model and reimage the underlying pre-exiting WAZ data (Roende, et al, 2020). A minimum 40 km offset for each node was acquired to ensure enough deep penetration.

In Figure 9, the left side shows the velocity models and the right side shows the corresponding RTM images; the upper row is the legacy model and corresponding image, and lower row is FWI model and corresponding image. These demonstrate several advantages and improvements over the legacy model. First, FWI can automatically modify the salt geometry. It also resolves the low-velocity gas clouds in the shallow part of the section, and significantly modifies the sediment velocity near the salt, which is typically challenging for ray-based tomography to resolve. Also, the FWI velocity model follows the geological structure quite well. Comparing the RTM images, after FWI the subsalt image focusing and coherency is much improved, and the most striking image improvement is that FWI can heal the disrupted event, which is caused by the wrong velocity model near the salt flank.

Figure 10 shows the comparison of the LSRTM image and FWI imaging, based on the same FWI velocity model. FWI imaging better resolves the sediment events towards the salt boundary termination. This could be due to FWI using all the propagation modes including diving wave and multiples, in addition to the reflection mode, which therefore illuminates the subsalt area better. The FWI image is cleaner and shows a more broadband image, which could be attributed to several reasons: the multi-frequency/scale FWI approach enhances the low-frequency content, helping to suppress the sidelobes of the source wavelet and secondly FWI estimates the source wavelet more effectively, therefore it has a source wavelet deconvolution effect during the iterative data-fitting process. The FWI image is without a ghosted source wavelet, but in RTM the source wavelet is embedded in the image.

OBN survey in shallow water North Sea: A dense OBN survey was acquired by BP in 2017 over the Clair field in North Sea, with a source sampling of 25 m x 25 m, and receivers spaced at 50 m x 100 m.

Figure 11 shows the effectiveness of the FWI process as a velocity model update tool. Comparing the initial model (top left) to the updated model after FWI (top right), FWI can effectively resolve the shallow high-resolution high-velocity anomalies; note that it also changes the deeper velocity structure quite significantly. Moreover, the high-resolution velocity model derived by FWI clearly improves the RTM-migrated section as shown in the bottom-right pane: events below the shallow high-velocity anomalies are flatter and more focused, with deeper reservoir events being less wavy and better focused compared to the corresponding RTM-migrated section, which was obtained using the initial model (bottom left)

Figure 12 shows the comparison between RTM and FWI-imaging. The left pane shows the result obtained via RTM and the right pane shows the result obtained via FWI imaging, where the final FWI velocity model shown in Figure 11 was used in both cases. Comparing the FWI imaging result with the RTM result, we see that FWI imaging clearly provides additional clarity and sharpness. Moreover, FWI imaging has less migration artifacts and a higher S/N. Most importantly, FWI imaging shows more subtle information at the reservoir level, including details which appear to be altogether absent from the regular RTM result.

Conclusions

LSRTM provides better image quality compared to conventional RTM. Two different types of LSRTM algorithms exist in the industry, each serving a different purpose. Single iteration

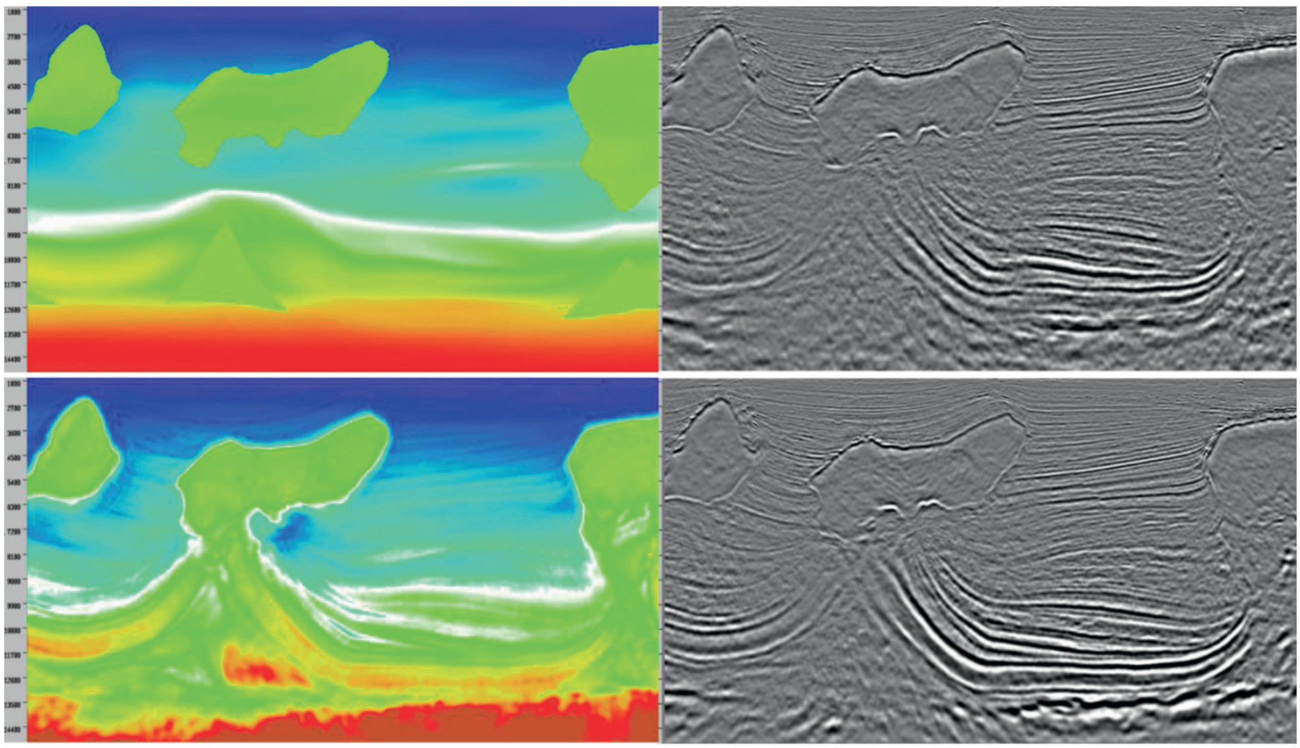

Figure 9 Left figures: velocity model. right figures: Corresponding RTM images. Upper pictures are before FWI and bottom pictures are after FWI.

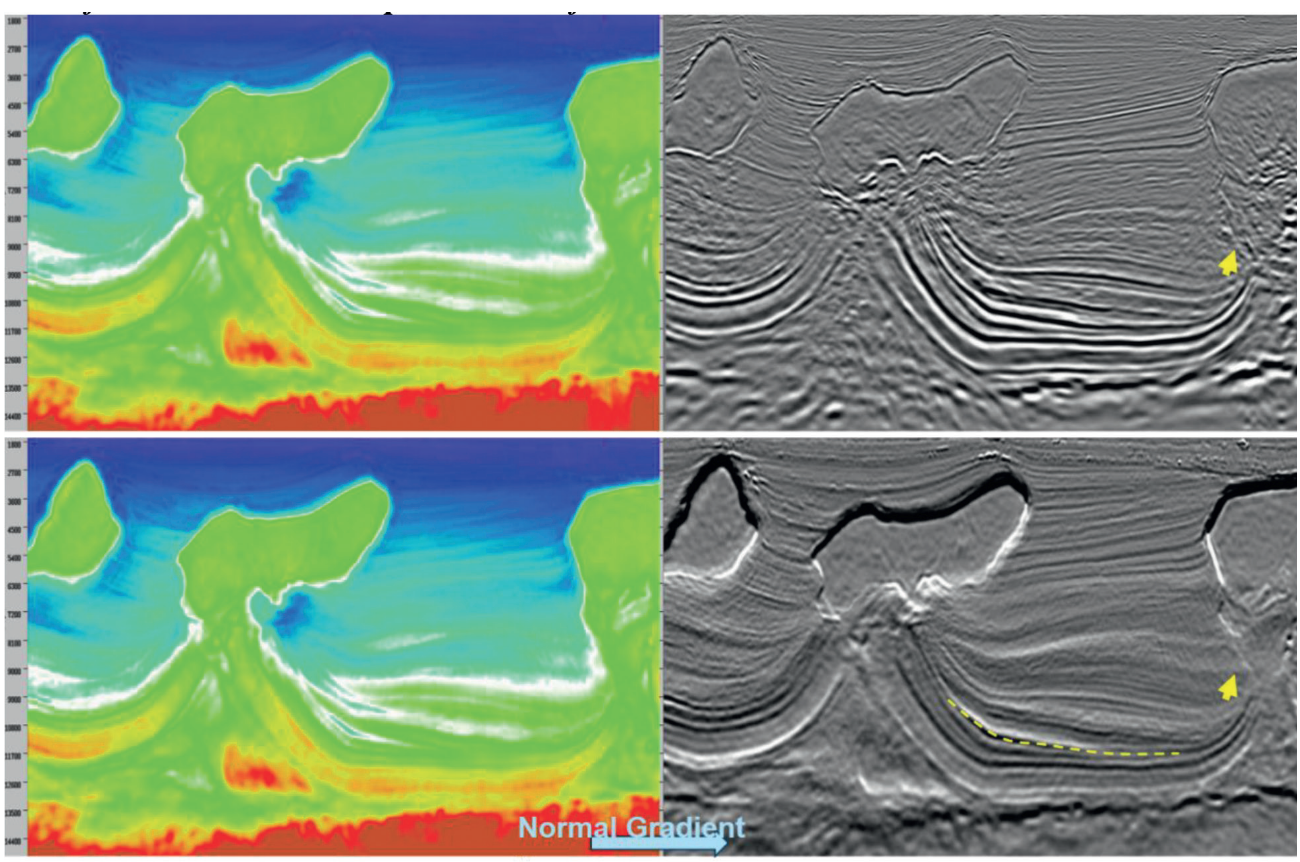

Figure 10 Left figures are the velocity model. Upper right is LSRTM image and bottom right is FWI image.

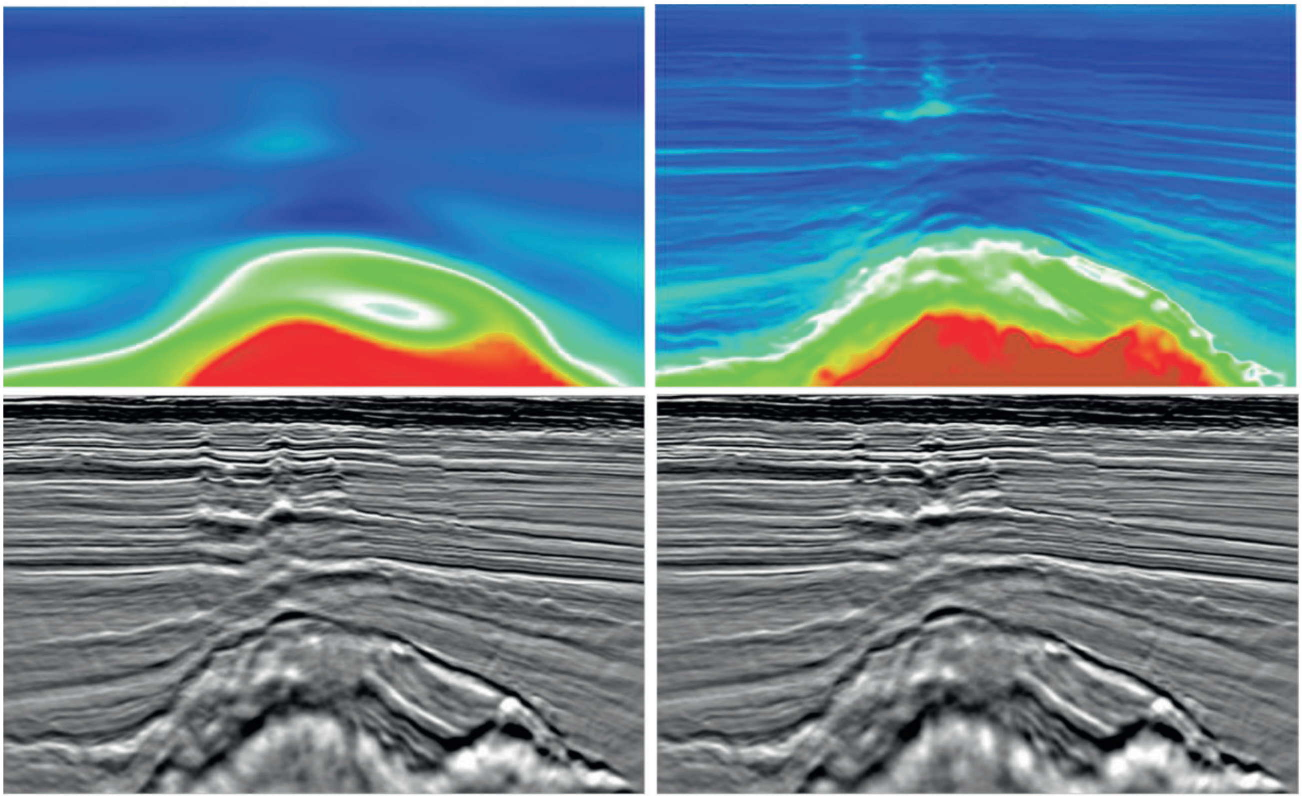

Figure 11 Upper row shows the velocity models. Bottom row shows the corresponding RTM images. Left side is for initial velocity model. Right side is after FWI update.

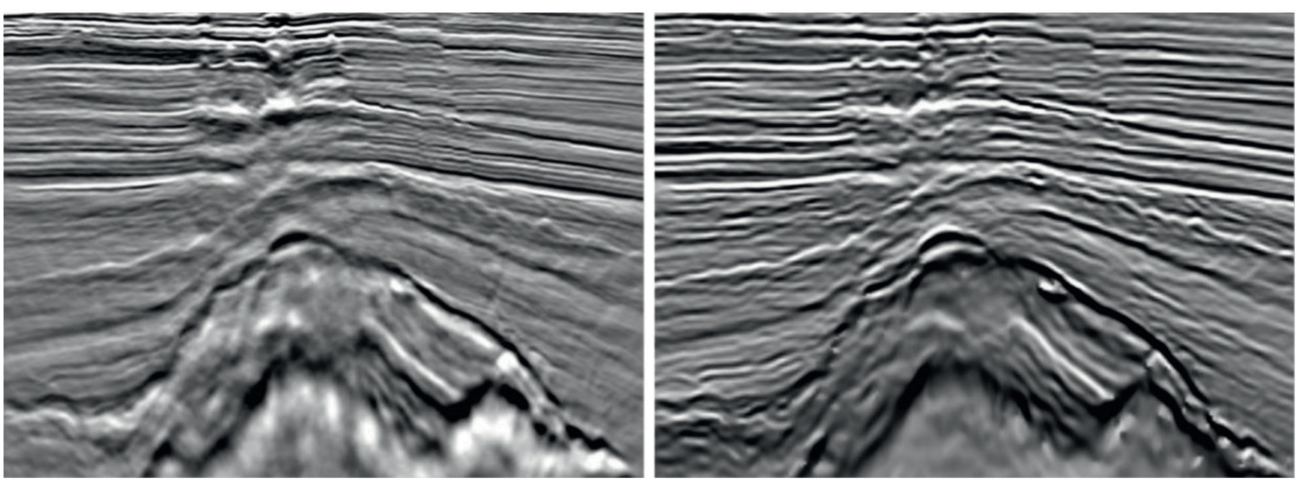

Figure 12 Comparison of regular RTM image vs FWI imaging based on the same final FWI velocity model. Left: Regular RTM image. Right: FWI imaging.

image-domain LSRTM is efficient and can effectively compensate for illumination, can improve amplitude fidelity, and is generally more suitable for generating AVO-friendly gathers. Data-domain LSRTM is an iterative approach which tends to broaden the spectrum and improves event focusing and resolution. Despite offering the above benefits, LSRTM carries the limitation that it is a linear inversion algorithm, and so requires a highly-accurate velocity model.

With the convergence of LSRTM and FWI, FWI is starting to extend its applicability beyond velocity updating into the realm of direct structural imaging through the FWI imaging process. Comparing FWI imaging with data-domain LSRTM, the former tool can be viewed as a natural extension of the latter. Specifically, FWI imaging is a non-linear inversion-based variant of data-domain LSRTM, which carries many advantages: robustness with respect to initial velocity model errors, the ability to use the full wavefield (i.e., diving waves and primary and multiple reflections), and improved efficiency in its use of multi-frequency bands. It is conceivable that the industry may eventually be able to replace the conventional processing flow with a single step of FWI imaging.

Acknowledgements

We would like to thank TGS and its partner WesternGeco, BP and its Clair partners: Shell, Chevron and Harbour Energy for permission to publish this work. Many TGS colleagues have contributed to the work shown here, and in particular we thank the following people for their contributions and support: Shuqian Dong, Chong Zeng, James Sheng, Xing Hao, Cheng

Cheng, Seet Li Yong, Sarah Spoors, Henrik Roende, Duncan Bate, Duncan Woolmer, and Adriana Citlali Ramirez.

References

Cheng, C., He, Y., Mao, J. and B. Wang, [2020]. Structure constrained least-squares migration of total reflection and its application, SEG Technical Program Expanded Abstracts: 3832-3835.

Dai, W., and Schuster, G.T. [2009]. Least-squares Migration of Simultaneous Sources data with a Deblurring Filter. SEG Technical Program Expanded Abstracts: 2990-2994.

Dai, W., Huang, Y. and Schuster, G.T. [2013]. Least-squares reverse time migration of marine data with frequency-selection encoding. *Geophysics*, **78**(4), S233-S242.

Dong, S., Cai, J., Guo, M., Suh, S., Zhang, Z., Wang, B. and Li, Z. [2012]. Least-squares reverse time migration: towards true amplitude imaging and improving the resolution, SEG Technical Program Expanded Abstracts: 1488.1-5.

Fletcher, R.P., Nichols, D., Bloor, R. and Coates, R.T. [2016]. Least-squares migration – Data domain versus image domain using point spread functions: *The Leading Edge*, **35**, 157-162.

He, Y., Hao, F., Dong, S. and Wang, B. [2018]. Towards AVO Compliant Least Squares RTM Gathers, SEG Technical Program Expanded Abstracts: 4408-4412.

He, Y., Xing, H., Huang, Y., Liu, F. and Wang, B. [2021]. Inversion-based Imaging: FWI beyond Velocity. EAGE 82nd Conference and Exhibition

Huang, R., Zhang, Z., Wu, Z., Wei, Z., Mei, J. and Wang, P. [2021]. Full-waveform inversion for full-wavefield imaging: Decades in the making, *The Leading Edge*, **40**(5), 324-334.

Lu, R., Lazaratos, S., Hughes, S. and Leslie, D. [2016]. Revealing overburden and reservoir complexity with high-resolution FWI, SEG Technical Program Expanded Abstr*acts*: 1242-1246.

Lu, S., Liu, F., Chemingui, N. and Orlovich, M. [2018]. Full wavefield migration by inversion, SEG Technical Program Expanded Abstracts: 4311-4315.

Ma, Y. and Hale, D. [2013]. Wave-equation reflection traveltime inversion with dynamic warping and full-waveform inversion: *Geophysics*, **78**(6), R223-R233.

Ma, Y., Hale, D., Gong, B. and Meng, Z. [2012]. Image-guided sparse-model full waveform inversion: *Geophysics*, **77**(4), R189-R198.

Mao, J., Sheng, J., Huang, Y., Hao, F. and Liu, F. [2020]. Multi-Channel dynamic matching full-waveform inversion: SEG Technical Program Expanded Abstracts, 666-670.

Michell, S., Shen, X., Brenders, A., Dellinger, J., Ahmed, I. and Fu, K. [2017]. Automatic velocity model building with complex salt: Can computers finally do an interpreter's job?: 87th Annual International Meeting, SEG, Expanded Abstracts, 5250-5254.

Nemeth, T., Wu, C. and Schuster, G.T. [1999]. Least-squares migration of incomplete reflection data, *Geophysics*, **64**(1), 208-221.

Pratt, R.G., Shin, C. and Hicks, G.J. [1998]. Gauss-Newton and full Newton methods in frequency-space seismic waveform inversion: *Geophysical Journal International*, 133, 341-362.

Roende, H., Bate, D., Mao, J., Huang Y. and Chaikin, D. [2020]. New node acquisition design delivers unprecedented results with Dynamic Matching FWI – case study from the Gulf of Mexico, *First Break*, 73-78.

Routh, P., Neelamani, R., Lu, R., Lazaratos, S., Braaksma, H., Hughes, S., Saltzer, R., Stewart, J., Naidu, K., Averill, H., Gottumkkula, V., Homonko, P., Reilly, J. and Leslie, D. [2017]. Impact of high-resolution FWI in the Western Blank Sea: Realing overburden and reservoir complexity, *The Leading Edge*, **36**(1), 60-66.

Sheng, J., Leeds, A., Buddensiek, M. and Schuster, G.T. [2006]. Early arrival waveform tomography on near-surface refraction data: *Geophysics*, **71**(4), U47-U57.

Shin, C. and Cha, Y.H. [2009]. Waveform inversion in the Laplace-Fourier domain: *Geophysical Journal International*, 177, 1067-1079.

Schuster, G.T. [1993]. Least-squares cross-well migration: SEG Technical Program Expanded Abstracts, 110-113.

Tang, Y. [2009], Target-oriented wave-equation least-squares migration/inversion with phase-encoded Hessian, *Geophysics*, **74**(6), WCA95-WCA107.

Tarantola, A. [1984]. Inversion of seismic reflection data in the acoustic approximation: *Geophysics*, 49, 1259-1266.

Verschuur, D.J., Staal, X.R. and Berkhout, A.J. [2016]. Joint migration inversion: Simultaneous determination of velocity fields and depth images using all orders of scattering, *The Leading Edge*, **35**(12), 1037-1046.

Virieux, J. and Operto, S. [2009]. An overview of full waveform inversion in exploration geophysics: *Geophysics*, **74**(6), WCC1-WCC26.

Wang, B. [2014]. EAGE E-lecture: Least Squares Reverse Time Migration by Bin Wang: https://www.youtube.com/watch?v=PZEHGpiZJAY.

Wang, B., He, Y., Cheng, C. and Liu, F. [2020]. Least Squares Migration in Complex Geology, SEG Technical Program Expanded Abstracts: Post-convention workshop 17.

Wang, P., Gomes, A., Zhang, Z. and Wang, M. [2016]. Least-sqaures RTM: Reality and possibities for subsalt imaging: SEG Technical Program Expanded Abstracts: 4204-4209.

Wang, P., Zhang, Z., Mei, J., Lin, F. and Huang, R. [2019]. Full-waveform inversion for salt: A coming of age, *The Leading Edge* 38: 204-213.

Warner, M., Ratcliffe, A., Nangoo, T., Morgan, J., Umpleby, A., Shah, N., Vinje, V., Štekl, I., Guasch, L., Win, C., Conroy, G. and Bertrand, A. [2013]. Anisotropic 3D full-waveform inversion: *Geophysics*, **78**(2), R59–R80, doi: 10.1190/geo2012-0338.1.

Warner, M. and Guasch, L. [2016]. Adaptive waveform inversion. Theory, *Geophysics*, **81**(6): R429-R445.

Wong, M., Biondi, B. and Ronen, S. [2014]. Imaging with multiples using least-squares reverse time migration: *The Leading Edge*, **33**(9), 970-976.

Wu, R., Luo, J. and Wu, B. [2014]. Seismic envelope inversion and modulation signal model: *Geophysics*, **79**(3), WA13-WA24.

Xing, H., He, Y., Huang, Y. and Sheng, J. [2020]. Ultralong Offset OBN: Path to better subsalt image, SEG Technical Program Expanded Abstracts: 2938-2942.

Yu, J., Lewis, L.J., Katz, J., Followill, F., Sun, H. and Schuster, G.T. [2003]. Autocorrelogram migration: IVSPWD test, *Geophysics*, **68**(1), 297-307.

Zeng, C., Dong, S. and Wang, B. [2014]. Least-squares reverse time migration: Inversion-based imaging toward true reflectivity, *The Leading Edge* 33: 962–964, 966, 968.

Zeng, C., Dong, S. and Wang, B. [2016]. Adaptive least-squares RTM with applications to subsalt imaging: *The Leading Edge*, **35**(3), 253-257.

Zhang, Y., Duan, L. and Xie, Y. [2015]. A stable and practical implementation of least-squares reverse time migration: *Geophysics*, **80**(1), V23-V31.

Zhang, Y., Ratcliffe, A., Roberts, G. and Duan, L. [2014]. Amplitude-preserving reverse time migration: From reflectivity to velocity and impedance inversion, *Geophysics* **79**(6), S271-S283.

Zhang, Z., Wu, Z., Wei, Z., Mei, J., Huang, R. and Wang, P. [2020]. FWI imaging: Full-wavefield imaging through full-wavefield inversion, SEG Technical Program Expanded Abstracts: 656-660.